DYNAMIC DATA ACQUISITION, REDUCTION, AND ANALYSIS FOR THE IDENTIFICATION OF HIGH-SPEED COMPRESSOR COMPONENT POST-STABILITY CHARACTERISTICS

S.D. Dvorak*, W.M. Hosny**, W.G. Steenken†
Aircraft Engine Business Group
General Electric Company
Cincinnati, Ohio 45215

and

J.H. Taylor‡
Corporate Research and Development
General Electric Company
Schenectady, New York 12345

ABSTRACT

A compressor test was conducted in which transient data were obtained for the purpose of identifying the high-speed post-stability characteristics. The transient, surge-cycle nature of high-speed post-stability operation precludes the possibility of obtaining the characteristics in a steady-state manner, as is possible during low-speed poststability operation, which is characterized by quasi-steady rotating-stall behavior. Specialized compressor instrumentation was developed and was used to obtain the necessary surge-cycle performance data, which were then digitized, filtered, and analyzed. The high-speed post-stability characteristics were obtained through the use of a maximum likelihood-parameter estimation technique. The estimated characteristics were found to be insensitive to the presence of measurement noise and unmodelled system dynamics, but the compressor time-response constants, which were also estimated, were more sensitive to these same disturbances.

NOMENCLATURE

A	-	Area
C_z	-	Axial Velocity
C_p	-	Specific Heat at Constant Pressure
g	-	Gravitational Constant
M	-	Mach Number
N	-	Rotor Speed
N_c	-	Corrected Speed = $N/\sqrt{\theta}$
P	-	Total Pressure
R	-	Gas Constant
s	-	Estimation Model Input
T	-	Total Temperature
T_i	-	Measured Temperature
t	-	Time
U	-	Mean Rotor Velocity
W	-	Airflow
W_c	-	Corrected Airflow = $W\sqrt{\theta}/\delta$
γ	-	Specific Heat Ratio
δ	-	Standard Day Pressure Correction Factor = P/P_o
θ	-	Standard Day Temperature Correction Factor = T/T_o
τ	-	Time Constant
φ	-	Flow Function = C_z/U
ψ'_{QS}	-	Quasi-Steady Pressure Coefficient: $\psi' = \frac{2C_p g_c T_{T1}}{U^2}\left[\left(\frac{P_{T2}}{P_{T1}}\right)^{\frac{\gamma-1}{\gamma}} - 1\right]$
ψ_{QS}	-	Quasi-Steady Work Coefficient: $\psi = \frac{2C_p g_c T_{T1}}{U^2}\left[\frac{T_{T2}}{T_{T1}} - 1\right]$

*Engineer, Operability Technology, Member AIAA
**Senior Project Engineer, Operability Technology, Member AIAA
†Manager, Engine Operability, Associate Fellow AIAA
‡System Engineer, Control Technology Branch

Subscripts

k	-	Discrete Time Step
s	-	Static
o	-	Standard Condition
1	-	Quasi-Steady Inlet Condition
2	-	Quasi-Steady Exit Condition
25	-	Compressor Inlet Station
31	-	Compressor Diffuser Exit Station

INTRODUCTION

The increasing sophistication and complexity of aircraft engines and their control systems has created a demand for enhanced design tools with which design and off-design engine system aerodynamic performance may be predicted before any hardware is built, assembled, or tested. One such tool is the dynamic engine model, which must be capable of simulating a wide range of steady-state and transient conditions in order to aid in the design of the engine hardware and control system for off-design conditions. Very often, the off-design conditions to be explored occur during post-stability transients, during which the validity of the model must be preserved.

For this reason, compression-component tests have been run specifically for the purpose of determining and analytically describing the post-stability characteristics of compressors. The test, data acquisition, reduction, and analysis described here were conducted as part of an ongoing effort to improve post-stability modelling techniques.

The compressor used on this test was the NASA-sponsored Energy Efficient Engine (E^3) compressor, a 10-stage, high-pressure ratio, high-airflow machine. The compressor was tested in both low and high-speed post-stall regimes. Steady-state performance data, as well as dynamic data, were recorded during the low-speed portions of the testing, and dynamic data were recorded during the high-speed portion of the testing; however, due to the transient nature of the high-speed instabilities, steady-state performance measurements were not possible. The testing and analysis of the low-speed rotating stall data is discussed in References 1 and 2. This paper addresses the high-speed dynamic data and the information concerning high-speed post-stability performance contained therein.

DATA ACQUISITION

In order to obtain data useful in quantifying surge cycle behavior, specialized instrumentation was developed. This instrumentation was designed to detect high frequency pressure and temperature variations, as well as rapid airflow fluctuations in both the forward and reverse directions.

The instrumentation was also designed to minimize sensor error due to drift or temperature variations and, should error occur, a system to aid in error detection and calibration was implemented.

The airflow rakes used in this test were custom-designed for the E^3 compressor flowpath with the purpose of measuring rapidly changing forward or reverse flow at the compressor inlet and exit (Figure 1). Two rakes were located at plane 25 (Figure 2) to measure the inlet flow and two rakes were located at plane 31 just aft of the diffuser to measure the exit flow . On each rake, transducers were mounted at two immersions in order to measure both hub and tip airflow.

The airflow rakes contain five sensors each; four pressure transducers (two facing forward and two facing aft) and one aspirated thermocouple.

The pressure sensors are high response differential transducers which are mounted in a tube inside the rake; the end of this tube projects into the gas flowpath. When the dynamics of this tube are considered, the natural frequency of the pressure measurement becomes 400 Hz, well above the frequencies of interest in surge analysis. There is a leakage path around the transducer in the tube so that the tube pressure may be measured by another remotely mounted transducer. These remotely mounted transducers are used to measure the steady-state pressure in the tubes for calibration purposes.

The thermocouples were type E (chromel-constantan) for both plane 25 and plane 31. The thermocouple junctions were made 0.001 inches in thickness in order to give a time constant of 10 milliseconds. These thermocuples were mounted facing aft on the rakes and were normally aspirated. The temperature recovery for the probes was $T_i/T = 0.994$.

Since the sensitivity of the pressure transducer changes with temperature, the rakes themselves were kept at a constant temperature by means of fluid circulation. The plane 25 rakes were heated during the test by circulating sump oil at 100°F. The plane 31 rakes were water cooled to maintain a transducer temperature of less than 110°F.

To improve the accuracy of the pressure measurements, differential pressure transducers were chosen with ranges only large enough to measure expected pressure fluctuations about a

reference pressure level. The ZOC (Zero, Operate, and Calibrate) system was used to introduce a constant, accurately measured pressure to the reference side of the transducers so that the range of the transducers would be extended to the magnitude of pressure to be measured.

The ZOC system has three modes of operation; the "zero", "operate", and "calibrate" modes. The operate mode is the mode in which data are normally taken. The zero mode is used to pneumatically couple the sensing side of the transducers to the reference side such that the transducer output should be zero. In this mode, zero shift or electrical bias may be determined.

In the calibrate mode, a known differential pressure is applied to the reference side of the transducers. This mode is used to determine any changes in transducer sensitivity during the test due to changes in operating conditions such as temperature.

The reference pressure generated by the ZOC system was measured by high-accuracy absolute pressure transducers. The voltage output from these transducers was recorded on magnetic tape along with the voltage output of the airflow rake transducers. The ZOC pressure was also measured by the steady-state facility measurement system so that the airflow rake/ZOC system calibration procedure could be documented by steady-state readings.

Once the dynamic, in-surge data had been obtained, a few steps were necessary before the airflow calculations could be performed. First, the analog data, which was in the form of electrical signals, had to be digitized. Then, the actual pressures and temperatures had to be reconstructed from these digitized electrical signals.

During the test, the dynamic temperatures and pressures measured by the airflow rakes were recorded on analog tape. The test-facility data-measurement system amplified the DC voltage output of the pressure and temperature transducers. The tape recorder converted these voltages into FM signals.

During tape playback and digitization, the FM signals were reconverted to DC voltages, which in turn were amplified before being sent into the digitization system.

The digitization system consisted of an IBM PC XT configured with an analog-to-digital board and special software. The data was digitized on a 12-bit A-D convertor at a sampling rate which was set to 1000 samples/sec.

The calibration and airflow calculations were done on the IBM PC, with the final pressures, temperatures, and airflow then transmitted to a VAX mainframe computer for filtering and characteristic estimation.

The procedure for calibrating the airflow rake transducers involved recording two special steady-state data points during the test: a "zero" point and a "calibrate" point. While the compressor was in a steady-state operating condition, three consecutive steady-state readings would be taken: "zero", "calibrate", and "operate" points. This calibration procedure was sufficient to determine the sensitivity and bias for each transducer. However, before each surge playback, a near-stall steady-state data point was run to determine a DC bias setting so that the digital playback of the rake instrumentation matched the data recorded during the steady-state reading using the test facility instrumentation. For example, the forward-facing pressure-probes were adjusted to read the plane average total pressures. Likewise, the individual thermocouples were adjusted to read the plane average temperature as recorded by the facility instrumentation.

On each airflow rake are two pairs of forward and aft-facing pressure probes. During normal operation, the pressure measured on the forward facing probe is the total pressure of the airflow at that point, while the aft-facing probe will measure a lower pressure (the base pressure) which is slightly higher than the local static pressure. Because of the close proximity of these two probes, these forward and aft pressures can be used to calculate a local Mach number by the use of the following formula:

$$M_{CALC} = \sqrt{\frac{2}{\gamma-1}\left[\left(\frac{P_f}{P_a}\right)^{\frac{\gamma-1}{\gamma}} - 1\right]} \qquad (1)$$

Since the aft pressure measured is a "wake" pressure and not a true static pressure, an empirical formula is used to obtain the true Mach number from the calculated Mach number:

$$M_{TRUE} = a\, M_{CALC} + b \qquad (2)$$

where a and b are experimentally determined for each pair of pressure probes. This relationship can be obtained from a small flow calibration system. The corrected flow is then calculated as follows:

$$W_c = \frac{A\sqrt{T_o}}{P_o}\sqrt{\frac{\gamma_g}{R}}\;\frac{M_{TRUE}}{\left(1+\frac{\gamma-1}{2}M_{TRUE}^2\right)^{\frac{\gamma+1}{2(\gamma-1)}}} \qquad (3)$$

From this corrected flow, the physical flow can be calculated in the following manner:

$$W = W_c \frac{P}{P_o} \sqrt{\frac{T_o}{T}} \qquad (4)$$

where P and T are the total pressure and total temperature at the plane of airflow measurement. During a surge, reverse flow can also be measured, the total pressure being measured on the aft-facing probe and the wake pressure being measured on the forward facing probe. The wake pressure is always lower than the total pressure, thus the direction of the local airflow can be determined by calculating the direction of pressure drop across a probe pair.

DATA REDUCTION

The transient airflow rake measurements for four instabilities at three speeds (90%, 95%, and 98.5% corrected speed) were chosen for further reduction and analysis. In each of these cases, the primary instability mode was surge, a relatively low-frequency, "nearly-axisymmetric" performance fluctuation.

The flow measurement method used to obtain the unsteady, transient airflow rate during surges is particularly sensitive to flow and pressure variations which are not necessarily indicative of axisymmetric flow fluctuations. One of the major non-axisymmetric disturbances were rotating stall cells which were present in one form or another during all of the surge transients recorded during this test.

The presence of high frequency pressure fluctuations can readily be seen in the inlet pressure signal recorded during the 90% speed instability, as shown in Figure 3. In order to correctly analyze this signal in the frequency domain, the first order trend was removed from the signal. The resulting power spectral density of this signal is shown in Figure 4. Note the dominant high frequency peak at a frequency of 81.2 Hz. From interstage wall static pressure instrumentation, the rotating stall frequency was measured to be 82.5 Hz (see Reference 1). The peak just to the right of that peak is at approximately 162 Hz which would be the second harmonic of the fundamental rotating stall frequency. The low frequency peaks occur at 7 Hz and 16 Hz, and are more representative of the axisymmetric flow fluctuations in the compressor. In the planes of flow measurement upstream and downstream of the compressor, the flow patterns of interest are fluctuations resulting from axisymmetrical flow oscillations. The circumferential pressure disturbance caused by rotating stall cells distorts the planar flow measurements to the point of questionable physical significance. This type of disturbance must be eliminated or at least attenuated in order to be consistent with the level of sophistication inherent in a one-dimensional parameter estimation model.

It was therefore decided to filter the mass flow rate prior to its use in the estimation process. The Butterworth filter design option of the IDPAC software package was used because of its speed and compatibility with the parameter estimation routines. The IDPAC software package is documented in Reference 3. The filter cutoff frequency was chosen at 48 Hz, and third order and fifth order Butterworth filters were designed. Figure 5 shows the spectral densities of the pressure signals (1), filtered with a third order filter (3), and filtered with a fifth order filter (5).

These filtered pressures are then used to calculate local airflows, which are then arithmetically averaged to obtain the airflow at a given plane. Figure 6a shows a local compressor inlet airflow before and after filtering by this method, with the corresponding frequency domain plots shown in Figure 6b.

DATA ANALYSIS

Once the data had been filtered and the airflows calculated, the surge data could be examined. The results of the 98.5 percent corrected speed surge will now be discussed. Figures 7 and 8 show the compressor-pressure-ratio and inlet-airflow responses to the onset of instability.

The pressure ratio and airflow responses show that it took about 1.4 seconds after the initial instability until quasi-steady surge cycles were established. Figure 9 is a plot of compressor pressure ratio versus inlet airflow and shows the initial instability transient and subsequent surge cycles. The initial transient was affected by the significant initial flow reversal through the compressor interacting with the facility inlet refrigeration system and the inlet and exit ducts, which are shown in Figure 10. A description of these effects is given in Reference 1. It should be mentioned that as a result of this flow reversal which included not only the compressor discharge plenum, but also the facility exhaust volume, and the continuous pumping airflow from the inlet refrigeration units, a significant increase in inlet pressure and temperature resulted. Following the initial instability, blowdown, and surge cycle development, the compressor entered

a period of relatively stable surge cycles. These cycles are shown in Figure 11. The repetitive character of these cycles makes them ideal for use in estimating the in-stall compressor characteristics, which will be explained in the next section.

It is clear from Figure 9 that the recovery segments of the surge cycles do not recover to the pressure ratio and airflow of the initial stall point. It appears that the compressor is recovering, but at a much lower pressure ratio and airflow. Figures 12 and 13 point to a probable explanation. The compressor is run at a constant physical speed, and when the compressor inlet temperature increased during the initial transient, the corrected speed was driven down to between 70 percent and 80 percent. Analysis shows that when the compressor is run at low speeds with the stators in the high-speed position, the speed line and stall point is very close to that indicated by the in-surge recovery trajectories in Figure 11.

The pressure ratio and airflow were also calculated using the tip-probe pairs (Figure 14) and the hub-probe pairs (Figure 15). Comparing these two figures, one can see that the flow reversals during surge are not entirely axisymmetric. Rather, the flow at the tips of the blades breaks down and reverses to a much greater extent than the hub flow. This leads to a radial recirculation pattern which has been observed in other compressors.

Figures 16, 17, 18, and 19 show the inlet corrected airflow, inlet and exit-total pressure, and inlet total temperature, respectively, during these cycles as a function of time. From these plots, the characteristics of a surge cycle may be examined. A surge cycle starts at stall, at which time the exit pressure and flow rate drop significantly and the airflow actually reverses. The resulting flow blockage causes an initial sudden increase in the inlet pressure, followed by an equally sharp drop-off. Once in stall, the exit pressure and airflow remain at stable, in-stall levels. Interstage static pressure measurements indicate the presence of rotating stall cells during this phase (see also Reference 1). Also to be noted is the increase in inlet temperature during this in-stall phase, indicating some kind of flow reversal, probably at the tip. As the compressor recovers, the inlet temperature drops off, while exit pressure and airflow both increase before stalling again and beginning another surge cycle.

COMPRESSOR CHARACTERISTICS IDENTIFICATION

Problem Formulation

The oscillating, large amplitude nature of the surge cycle is described by a coupled set of highly nonlinear equations. Obtaining the high-speed in-stall characteristics from the instability dynamics by using these equations in this form is not feasible.

Many researchers, most notably Greitzer (Reference 4), have formulated an in-stall model which assumes that the various instability transients have as their forcing function a set of quasi-steady characteristics. The compressor can then be modelled such that the system non-linearities can be accounted for in the formulation of these quasi-steady characteristics, enabling the relationship between the quasi-steady and instantaneous characteristics to be modelled as a simple linear dynamic system.

When the compressor problem is thus decoupled into a quasi-steady non-linear part and a linear dynamic part, powerful statistical techniques based on estimation theory may be applied to the linear dynamic model to obtain both linear model parameter estimates and "fits" to the non-linear characteristics.

For this effort, Maximum Likelihood Parameter Estimation Theory (MLPET), applied via use of the software package IDPAC, was used to obtain estimates of the high-speed, in-stall, quasi-steady characteristics. This parameter estimation theory is described in Reference 5, and the capabilities and use of the IDPAC software are explained in Reference 3.

The dynamic model assumed for the compressor has as its foundation quasi-steady characteristics to which the compressor has two fundamental modes of response. This model is illustrated in Figures 20 and 21. The response shown in Figure 20 is associated with low-speed behavior and involves, at the point of stall, the transition from an unstalled steady-state point to a rotating stall quasi-steady operating point along a trajectory assumed to be a first order decay.

The high-speed post-stall transient is also assumed to be a first order response, but in this case the operating point migrates with time and the resulting surge cycle is therefore based at times on the in-stall characteristic, the unstalled characteristic, and also the in-stall reverse-flow characteristic. The high-speed operating point migration shown in Figure 21 may be compared with actual test data previously shown in Figures 9 and 11.

The techniques developed for identifying the in-stall characteristics corresponding to surge transient data are based on the fact that compressor flow exit properties can be related to the inlet conditions, and this relation is basically a function of the quasi-steady, in-stall characteristics and the compressor time-response constants. Evaluation of this relationship is done using only inlet and exit measurements. Thus, independent from the environment where the data are to be acquired, engine or test rig system, the identification process does not have to be system dependent. This approach simplified the identification methodology and alleviates many of the difficulties that would be encountered if the component parameter identification were based on a total system representation. In Reference 6, a methodology based on a total system identification model has shown that precise surge initiation synchronization between the model and the measurements was necessary for successful parameter identification. Such synchronization is expected to become more difficult when the surge is not initiated as a planar wave, as is the case with real compressors. In addition, for a system modelling technique, the compressor parameter estimation will be biased due to any errors introduced through incorrect modelling or misrepresentation of the other system components.

The pressure coefficient model structure is based on a simplified version of the momentum equation together with a first-order time-delay equation. A one-dimensional model was assumed, and the convective momentum terms and mass accumulation within the compressor control volume were neglected. With these assumptions, the momentum equation becomes decoupled from the mass and energy equations. Thus, the pressure coefficient can be explicitly obtained. The pressure coefficient may be denoted as functions of the inlet airflow derivative and inlet and exit pressures:

$$\Psi' = \Psi\left(\frac{dW_{25}}{dt},\ P_{25},\ P_{31}\right) \tag{5}$$

The first order time delay function is

$$\tau \frac{d\Psi'}{dt} + \Psi' = \Psi'_{QS} \tag{6}$$

where Ψ'_{QS} is the quasi-steady pressure coefficient and is a function of the flow coefficient φ. The flow coefficient is a function of the inlet measurements:

$$\varphi = \varphi(W_{25},\ P_{25},\ T_{25}) \tag{7}$$

For this model, the measured parameters are compressor inlet total pressure P_{25}, exit total pressure P_{31}, inlet total temperature T_{25}, and inlet physical airflow W_{25}. The pressure coefficient estimation model is discussed in more detail in Reference 7.

The pressure coefficient model estimation involves obtaining the time constant τ and the functional relationship between Ψ'_{QS} and φ. If one has suitable a priori information about the form of this relation, then it can be expressed in the form:

$$\Psi'_{QS}(\varphi) = \sum_{i=1}^{m} \beta_i s_i(\varphi) \tag{8}$$

where s_i comprise a set of known functions of φ and β_i are the unknown parameters to be estimated. The assumed functional form of Ψ'_{QS} (e.g., a polynominal in φ) dictates the set of signals s_i to be used. The relation described in Equation 8 is thus constrained to be a linear function of the signals s_i.

The model given by Equations 5 and 6 must be put into a discrete multi-input single-output (MISO) form for IDPAC to use:

$$\Psi'_{k+1} - a\,\Psi'_k = \sum_{i=1}^{m} b_i s_{i,k} \tag{9}$$

The coefficients for this model are

$$a = e^{-h/\tau} \tag{10}$$

and

$$b_i = (1-a)\,\beta_i \tag{11}$$

where h is the sample period. With the system in this form, the parameters to be estimated are a and b_i.

From previous estimation work on model data and low-speed in-stall test data, the in-stall pressure coefficient is assumed to be in the form of a parabola. Thus Equation 8 becomes

$$\Psi'_{QS} = b_1 s_1 + b_2 s_2 + b_3 s_3 \tag{12}$$

where $s_1 = 1.0$, $s_2 = \varphi$, and $s_3 = \varphi^2$

The work coefficient model structure is based on the compressor control volume energy equation together with a first order time delay equation. The time delay equation is similar in form to Equation 6. In addition to the measured variables required to estimate the pressure coefficient, the work coefficient model requires the compressor exit physical airflow rate W_{31}:

$$\Psi = \Psi\left(W_{25}, \frac{dW_{25}}{dt}, P_{25}, T_{25}, P_{31}, W_{31}\right) \tag{13}$$

The IDPAC estimation model formulation for the work coefficient follows the formulation for the pressure coefficient model (see Equations 8 through 11), except that the work coefficient was modelled as a series of piecewise linear segments with breakpoints δ_1 and δ_2 (Figure 22a) based on the known form of the low-speed in-stall work coefficient as described in Reference 2. This estimation model form is described by the following equation:

$$\Psi_{QS} = b_1 s_1 + b_2 s_2 + b_3 s_3 + b_4 s_4 \qquad (14)$$

where the input functions s_i are defined as shown in Figure 22. The work coefficient estimation model is discussed in more detail in Reference 7.

Model Identification for 98.5% Corrected Speed

The first case to be estimated was the 98.5 percent corrected speed case. However, before the estimation could be accomplished, two preliminary steps had to be taken to prepare the data. The first step was to obtain a segment of data during which the surge cycles were well developed and uniform. The second step was to segment the data into in-stall and unstalled regions. Figure 11 shows that the cycles can be separated into unstalled and in-stall regimes by choosing as a criterion the passing of the corrected inlet airflow rate through a threshold of about 50 lbm per second. The data was then separated into intervals during which the airflow rate was below this value, which became the in-stall data, and intervals during which the airflow rate is above this value, which became the unstalled data. (A study on data segmentation was performed in which it was found that the quality of estimation was quite insensitive to using the exact value of 50 lbm per second, or to the existence of hysteresis. These intervals were then linked to form an in-stall time series and an unstalled time series. The estimation process was then performed on the in-stall time series.

Figure 23 shows the estimated 98.5 percent corrected speed quasi-steady in-stall pressure coefficient. In order to compare the estimated in-stall pressure coefficient to the available steady-state in-stall data, some steady-state data points obtained during 75 percent corrected speed rotating-stall are included in the figure. This comparison has some validity due to the fact, previously shown in Figures 12 and 13, that an increase in inlet temperature during the 98.5 percent speed instability actually drove the corrected speed down into the 75 percent range. Note that the estimated characteristic is lower than the steady-state data. In comparing the test data and the estimate, it should be noted that they correspond to different in-stall behavior modes. The steady-state data were obtained during low-speed rotating stall. The estimate, however, was obtained from high-speed surge data using a one-dimensional, axisymmetric compressor estimation model. Recently, Greitzer and Moore (Reference 8) have proposed an approximate theory which predicts a difference between the rotating stall and the axisymmetric surge characteristic, the surge characteristic being steeper and lower near the zero flow region. The data presented in Figure 23 seem to support this theory.

Note that this curve can only be considered a reliable estimate of the actual in-stall quasi-steady pressure coefficient over the range of high significant amplitude density of the flow coefficient as shown by the histogram of Figure 24. This flow coefficient range extends approximately from -0.025 to 0.175.

Applying Equation 10 to the estimated parameter 'a' yields a time constant of 243 milliseconds. From the period of oscillation seen in Figures 16 through 19, it can be clearly seen that this is not the time constant for which we are looking. Rather, the estimation process seems to have estimated a time constant in order to fit the system-dependent slow trends observed in the increasing inlet pressure and temperature observed in Figures 17 and 19, which were due to compressor/facility interactions.

Model Identification for 90% Corrected Speed

The estimation process was also performed on data from the 90% speed instability. In this case, sufficient data were available to estimate both the pressure and work coefficients. The work coefficient model requirement of having measurements of exit physical flow rate limited the available data to the 90 percent speed case. This is because at higher speeds the exit temperature went beyond the measurement limits set in the data acquisition system, and temperature is necessary in calculating physical airflow rate. Figure 25 shows the estimated pressure and work coefficients for this case. The existence of rotating stall cells throughout the transient obviated data segmentation into in-stall and unstalled regimes.

Note that there is a significant amount of reverse flow at the inlet, as the histogram of the flow coefficient for the 90% instability, Figure 26, indicates. However, this high amount of reverse flow is not seen at the exit, which implies a high degree of flow recirculation within the compressor itself. (This recirculation is also noted during the 98.5% speed case as

shown in Figures 14 and 15). For this reason, estimates of the 90% characteristics are valid primarily in the positive flow region, from a flow coefficient of 0.0 to 0.1.

The final test for validation of these estimates was to obtain a reconstruction of the output based on the estimated model. IDPAC was used to simulate the deterministic part (no process or measurement noise) of the estimated 90 percent corrected speed model. The fact that the 90% corrected speed data was not segmented allowed the reconstruction to be performed on a continuous set of data. A new time constant was then chosen for the estimation model used in the pressure coefficient reconstruction using trial and error. It was found that a time constant of 18 milliseconds yielded an acceptable reconstruction. Figure 27 is a comparison of the actual instantaneous pressure coefficient and its reconstruction based on the estimated model and the measured flow coefficient.

CONCLUSIONS AND RECOMMENDATIONS

The post-stall compressor test, data reduction, and in-stall compressor characteristic estimation effort documented in this report represents a new direction in compressor performance evaluation. This effort was of value not only because of the wealth of previously unobtainable high-speed post-stall data that were obtained, but also because of the lessons learned in conducting this sort of test and data analyses.

The airflow rake/ZOC system worked very well in providing compressor inlet and exit pressures, temperatures, and airflows of sufficient quality and resolution so as to allow credible parameter estimates. Nevertheless, improvements to the design of this instrumentation have been proposed, particularly modifications which will allow change-out of faulty airflow rake transducers with minimal test scheduling impact. Also, new data reduction systems are in development which will permit on-line data digitization and airflow calculations. In addition, compressor-rig test-system modifications will be made to minimize the effects of the facility systems and ducting on the post-stall transients. The use of the commercially available IDPAC software as a data management and reduction tool, particularly the data filtering and characteristics estimation routines, proved invaluable in developing the data analysis procedures.

In spite of the system dynamics superimposed on the post-stall compressor transients, estimates of high-speed pressure coefficients at 90 and 98.5 percent corrected speed and the work coefficient at 90 percent corrected speed were obtained. These estimates were validated by comparing them to the E^3 low-speed rotating stall characteristics. To our knowledge, this is the first time that both the post-stall pressure and work coefficients have been identified from the same set of experimental data. The difference between the low-speed and the high-speed characteristics are consistent with analytical predictions. Also, a reconstruction of the instantaneous pressure coefficient was obtained from the estimated quasi-steady pressure coefficient for the 90 percent speed case. One area of further work is time constant estimation. The estimation procedure yields a very large time constant based on low frequency compressor-facility interactions. Future efforts must address this problem, both to improve the estimation model to allow for decoupling system and compressor dynamics, and to modify the facility and test procedure so that these dynamic interactions may be minimized as much as possible prior to data reduction and characteristics estimation.

ACKNOWLEDGEMENT

The authors wish to acknowledge the support of the National Aeronautics and Space Administration Lewis Research Center for providing the opportunity to conduct this compressor aerodynamic-instability test program. The work presented in this paper represents some of the effort funded under the post-stall/in-stall option of contract NAS3-24-83 and the effort funded under Task 4 of contract NAS3-24211. These efforts were carried out under the technical cognizance and encouragement of Mr. R.D. Hager of the NASA Lewis Research Center Turbine Engine Branch.

REFERENCES

1. Hosny, W. M., Lenhardt, C. H., Lin, H. T., Lovell, R. C., and Steenken, W. G., "Energy Efficient Engine (ICLS/IOC) High Pressure Compressor Component Performance Report," NASA-Lewis Research Center, NASA CR-174955, August 1985.

2. Hosny, W.M., and Steenken, W.G., "Aerodynamic Instability Performance of an Advanced High-Pressure-Ratio Compression Component," AIAA-86-1619, June 1986.

3. Weislander, J., "IDPAC Commands - User's Guide," Report TFRT-3157, Dept. of Automatic Control, Lund Institute of Technology, Lund, Sweden, 1976.

4. Greitzer, E. M., "Surge and Rotating Stall in Axial Flow Compressors. Part 1: Theoretical Compression

System Model," ASME Paper No. 75-GT-9, November 1974.

5. Astrom, K. J., "Maximum Likelihood and Prediction Error Methods," Automatica 16, pp 551-574, 1980.

6. Nunes, K. B., and Rock, S. M., "Identification of Quasi-Steady Compressor Characteristics from Transient Data," NASA-Lewis Research Center, NASA CR-174685, September 1984.

7. Dvorak, S.D., Hosny, W.M., and Steenken, W.G., "E^{3}10C Compressor Test Analysis of High-Speed Post-Stall Data," NASA-Lewis Research Center, NASA CR-179521, October 1986.

8. Greitzer, E. M., and Moore, F. K., "A Theory of Post-Stall Transients in Axial Compression Systems: Part II - Application," ASME Paper No. 85-GT-172, March 1985.

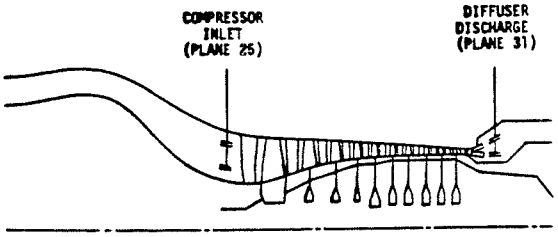

Figure 1. Dynamic Instrumentation Locations.

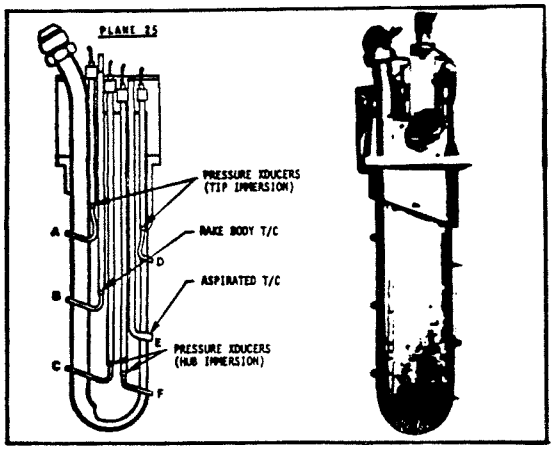

Figure 2. Plane 25 Transient Airflow Rake.

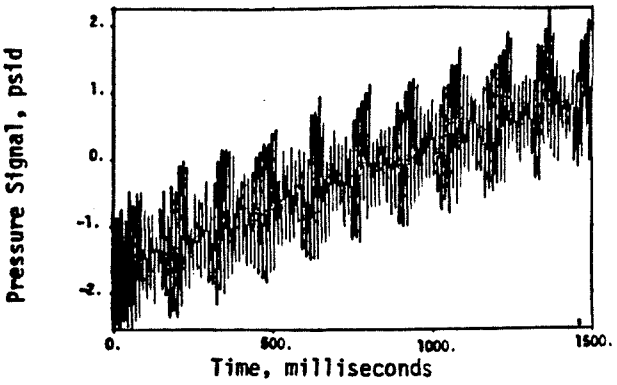

Figure 3. Unfiltered Inlet Total Pressure Signal, 90% Instability.

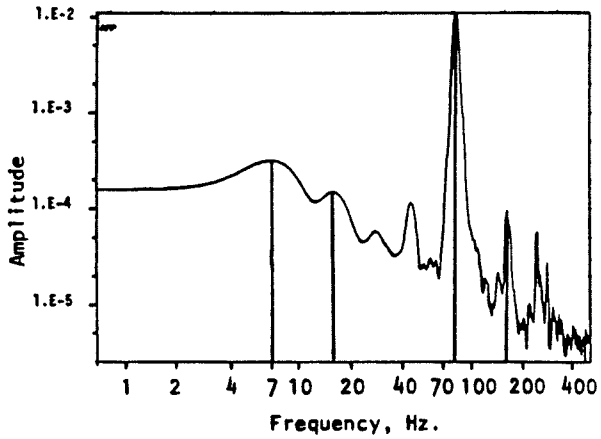

Figure 4. Power Spectrum of Unfiltered Pressure Signal with First Order Trend Removed, 90% N_C Instability.

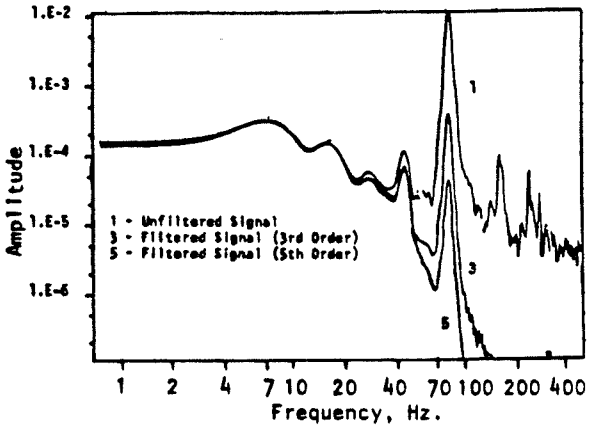

Figure 5. Power Spectra of Unfiltered and Filtered Inlet Total Pressure Signal, 90% N_C Instability.

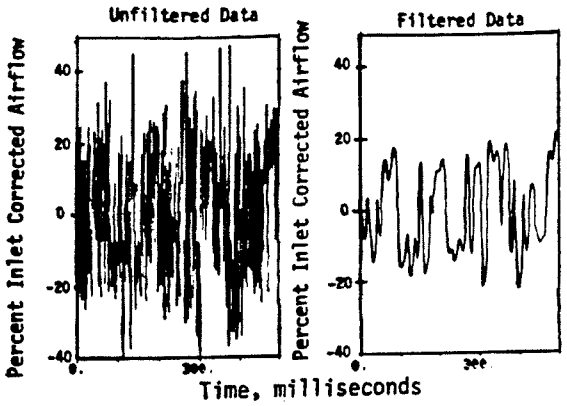

Figure 6a. A Comparison of Inlet Airflow Calculated from Unfiltered and Filtered Pressure Measurements, 90% N_c Instability.

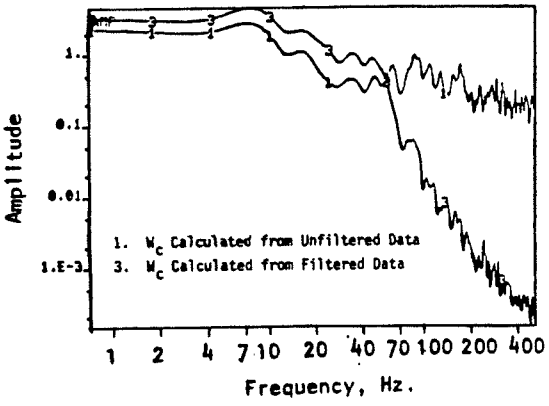

Figure 6b. Power Spectra of Inlet Airflow Calculated from Unfiltered and Filtered Pressure Measurements, 90% N_c Instability.

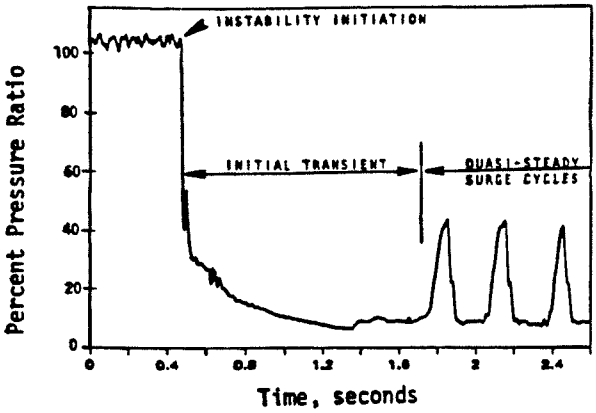

Figure 7. Face Average Pressure Ratio, 98.5% N_c Stall Inception.

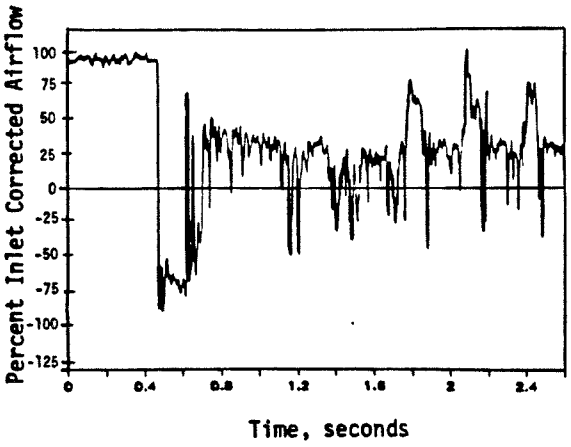

Figure 8. Face Average Inlet Corrected Airflow Rate, 98.5% N_c Stall Inception.

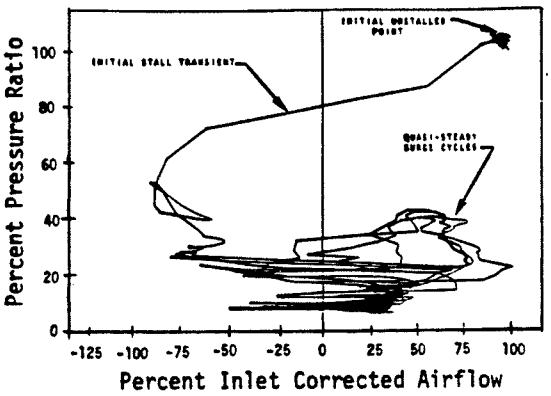

Figure 9. Operating Point Migration, 98.5% N_c Stall Inception.

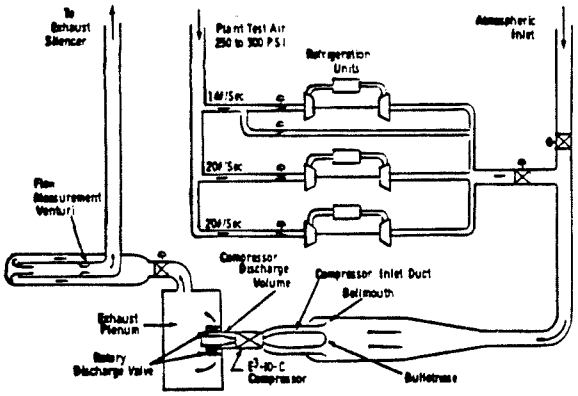

Figure 10. Test Facility Schematic.

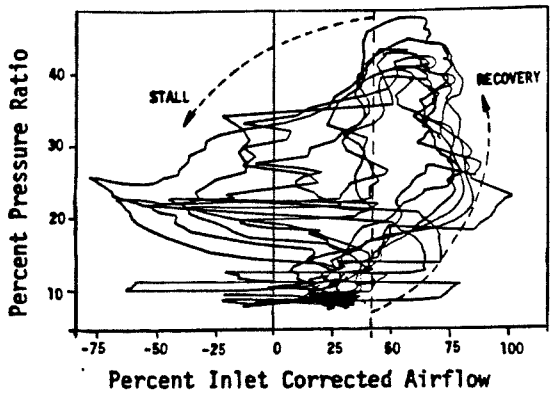

Figure 11. Operating Point Migration, 98.5% N_c Quasi-Steady Surge Cycles for 1.8<Time <3.6 Seconds.

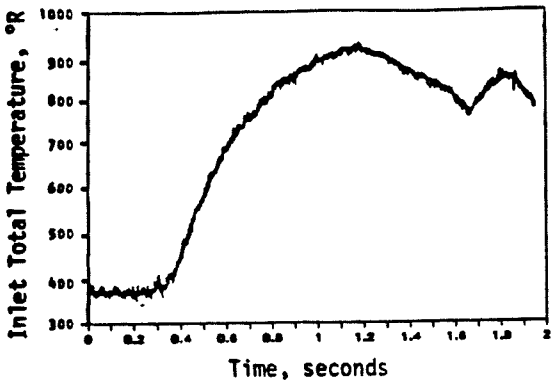

Figure 12. Compressor Inlet Total Temperature, 98.5% N_c Stall Inception.

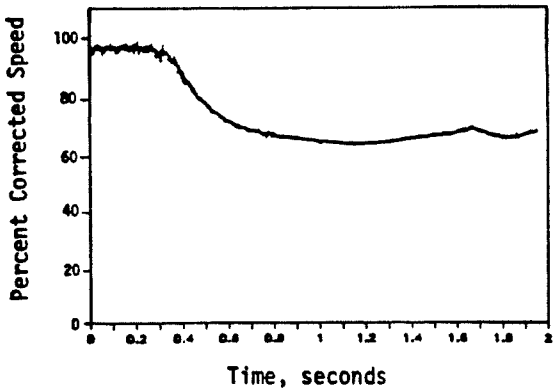

Figure 13. Compressor Corrected Speed, 98.5% N_c Stall Inception.

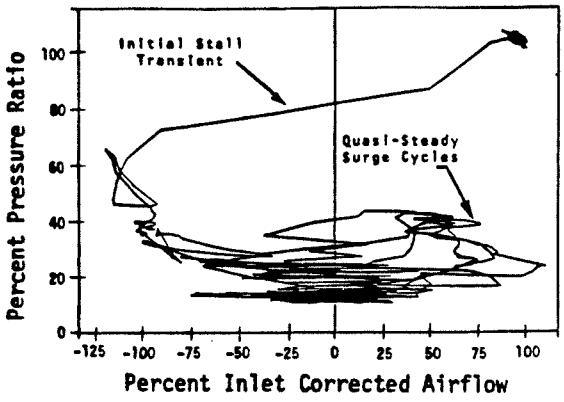

Figure 14. Tip Operating Point Migration, 98.5% N_c Stall Inception.

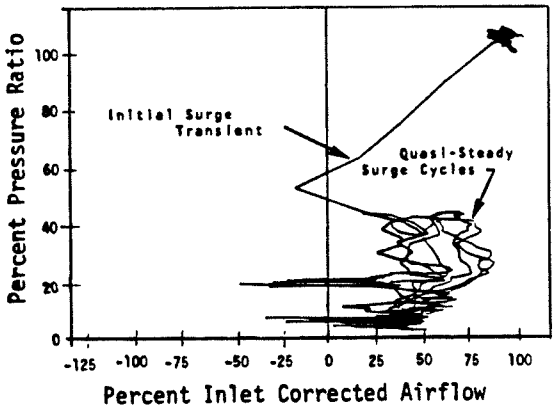

Figure 15. Hub Operating Point Migration, 98.5% N_c Stall Inception.

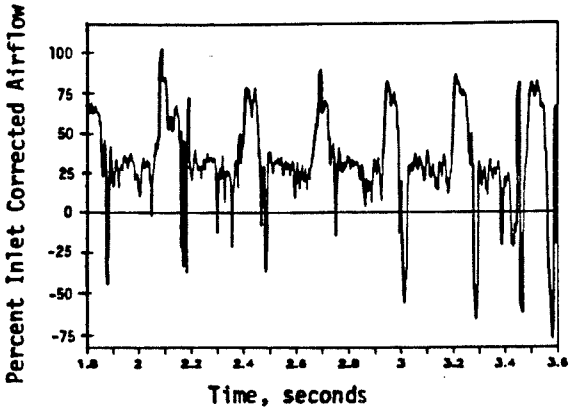

Figure 16. Inlet Corrected Airflow, 98.5% N_c Quasi-Steady Surge Cycles.

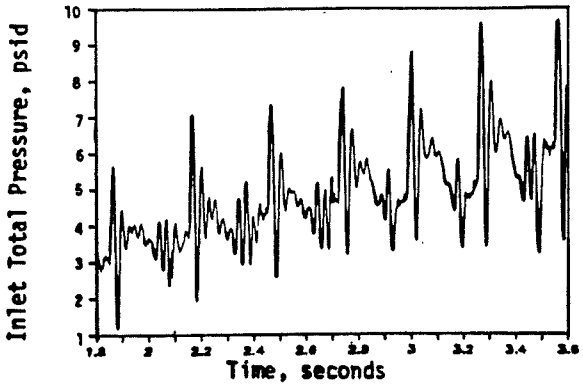

Figure 17. Inlet Total Pressure, 98.5% N_c Quasi-Steady Surge Cycles.

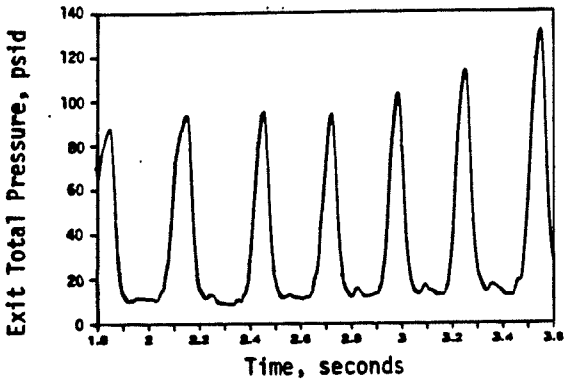

Figure 18. Exit Total Pressure 98.5% N_c Quasi-Steady Surge Cycles.

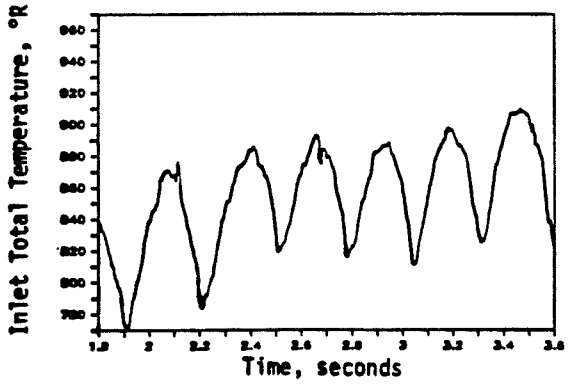

Figure 19. Inlet Total Temperature, 98.5% N_c Quasi-Steady Surge Cycles.

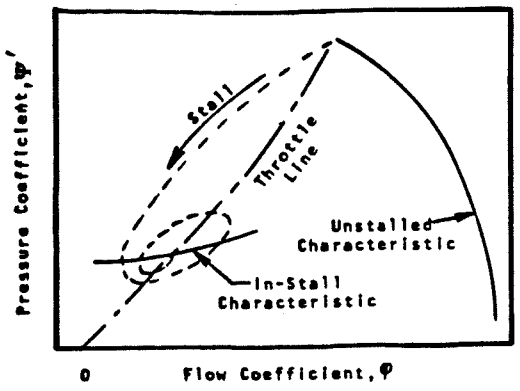

Figure 20. Low Speed Compressor Response.

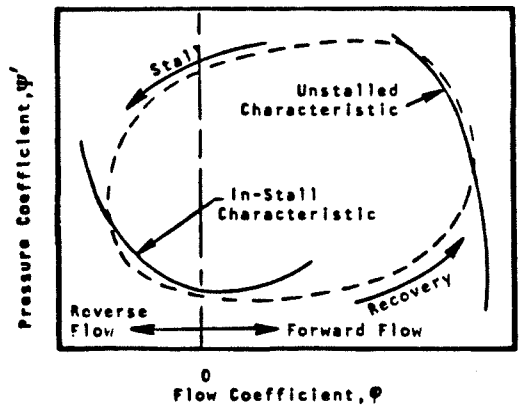

Figure 21. High Speed Compressor Response.

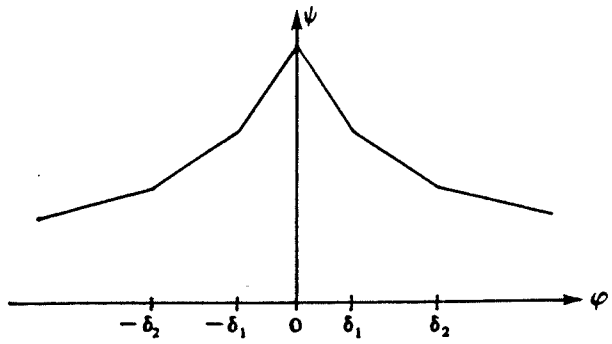

Figure 22a. Work Coefficient Estimation Model.

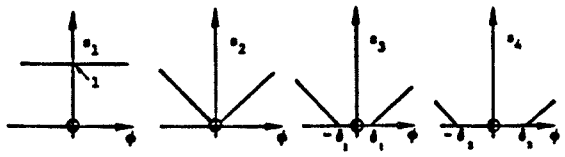

Figure 22b. Input Signals For Work Coefficient Estimation.

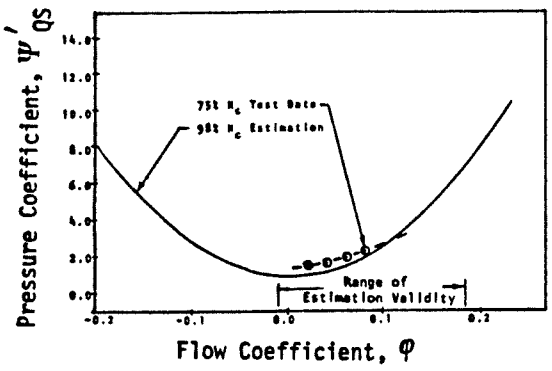

Figure 23. A Comparison Between the 98.5% N_c Estimated Pressure Coefficient and 75% N_c Test Data.

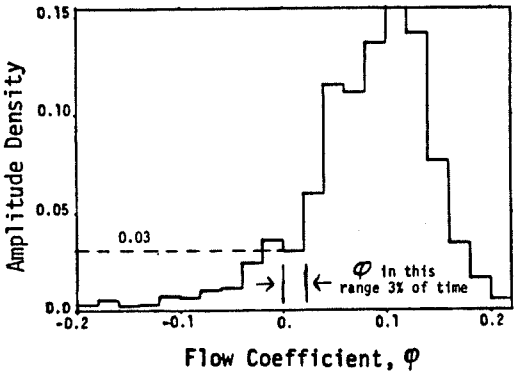

Figure 24. Histogram of In-Stall Flow Coefficient, 98.5% N_c.

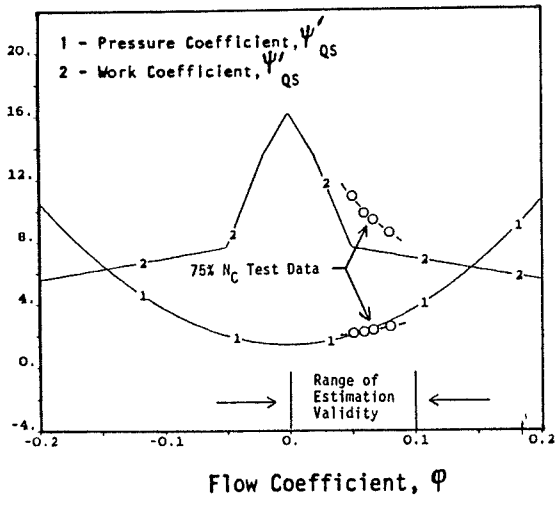

Figure 25. Pressure and Work Coefficient Estimation Model, 90% N_c.

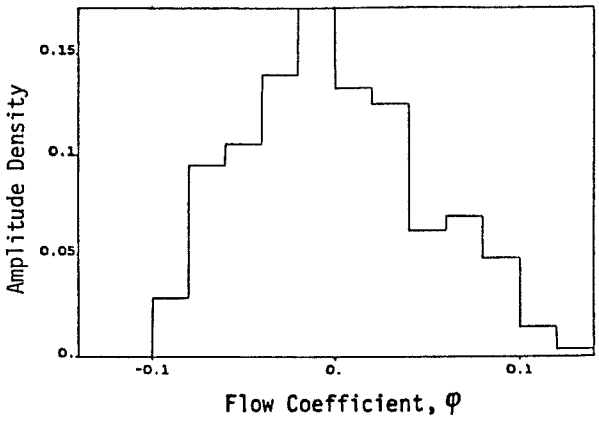

Figure 26. Histogram of the In-Stall Flow Coefficient, 90% N_c.

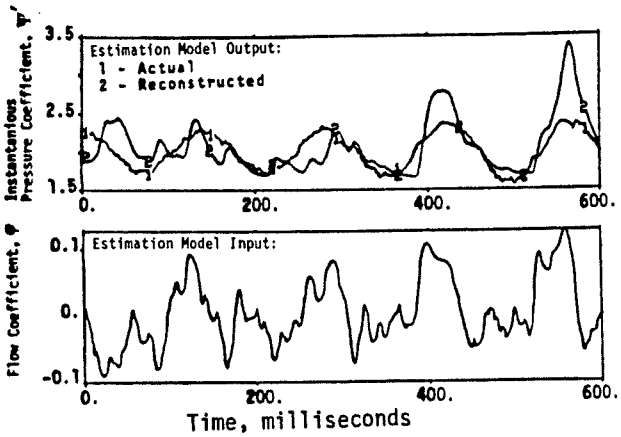

Figure 27. A Comparison of the Actual and Reconstructed Instantaneous Pressure Coefficient, 90% N_c.